



HAL
open science

Dynamic Mechanical Properties of a Biomimetic Hydroxyapatite/Polyamide 6,9 Nanocomposite

Cyril Sender, Eric Dantras, Lydia Laffont-Dantras, Marie-Hélène Lacoste-Ferré, Jany Dandurand, Monique Mauzac, Jean-Louis Lacout, Claudine Lavergne, Philippe Demont, Alain Bernès, et al.

► **To cite this version:**

Cyril Sender, Eric Dantras, Lydia Laffont-Dantras, Marie-Hélène Lacoste-Ferré, Jany Dandurand, et al.. Dynamic Mechanical Properties of a Biomimetic Hydroxyapatite/Polyamide 6,9 Nanocomposite. Journal of Biomedical Materials Research Part B: Applied Biomaterials, 2007, 83B (2), pp.628-635. 10.1002/jbm.b.30930 . hal-03481080

HAL Id: hal-03481080

<https://hal.science/hal-03481080v1>

Submitted on 15 Dec 2021

HAL is a multi-disciplinary open access archive for the deposit and dissemination of scientific research documents, whether they are published or not. The documents may come from teaching and research institutions in France or abroad, or from public or private research centers.

L'archive ouverte pluridisciplinaire **HAL**, est destinée au dépôt et à la diffusion de documents scientifiques de niveau recherche, publiés ou non, émanant des établissements d'enseignement et de recherche français ou étrangers, des laboratoires publics ou privés.



Open Archive Toulouse Archive Ouverte (OATAO)

OATAO is an open access repository that collects the work of Toulouse researchers and makes it freely available over the web where possible.

This is an author-deposited version published in: <http://oatao.univ-toulouse.fr/>
Eprints ID : 2629

To link to this article :

URL : <http://dx.doi.org/10.1002/jbm.b.30930>

To cite this version : Sender, C. and Dantras, Eric and Laffont-Dantras, Lydia and Lacoste-Ferré, M.-H. and Dandurand, Jany and Mauzac , M. and Lacout , Jean-Louis and Lavergne, C. and Demont , Philippe and Bernès, Alain and Lacabanne, Colette (2007) *[Dynamic Mechanical Properties of a Biomimetic Hydroxyapatite/Polyamide 6,9 Nanocomposite](#)*. Journal of Biomedical Materials Research Part B: Applied Biomaterials, vol. 83B (n° 2). pp. 628-635. ISSN 1552-4973

Any correspondence concerning this service should be sent to the repository administrator: staff-oatao@inp-toulouse.fr

Dynamic Mechanical Properties of a Biomimetic Hydroxyapatite/Polyamide 6,9 Nanocomposite

C. Sender,^{1,2} E. Dantras,¹ L. Dantras-Laffont,³ M. H. Lacoste,¹ J. Dandurand,¹ M. Mauzac,⁴ J.-L. Lacout,⁵ C. Lavergne,² Ph. Demont,¹ A. Bernès,¹ C. Lacabanne¹

¹ L2P, Institut CARNOT-CIRIMAT, Université Paul Sabatier, 31062 Toulouse, France

² TEKNIMED, 12 rue Apollo, 31240 L'Union, France

³ LRCS, Université Jules Verne, 80039 Amiens, France

⁴ IMRCP, Université Paul Sabatier, 31062 Toulouse, France

⁵ Institut CARNOT-CIRIMAT, ENSIACET, 31077 Toulouse, France

DOI: 10.1002/jbm.b.30930

Abstract: A biomimetic composite of nanohydroxyapatite (nHap) and semicrystalline polyamide 6,9 (PA 6,9) was synthesized by thermally induced phase separation. The nHap powder was dispersed in a polymer matrix with a low ratio ranging 1–10 wt %. The mean size of the nHap, determined by scanning electron microscopy (SEM) was ~100–200 nm (length), 40–60 nm (width). Physicochemical analyses were performed in order to characterize the PA 6,9 and nHap separately on the one hand, and the PA 6,9/nHap composites on the other hand. Differential scanning calorimetry (DSC) and dynamic mechanical analyses (DMA) have pointed out an optimization of the composite physical properties as a function of nHap content till a limit value of 5 wt %. Above this value, the mechanical properties decreased. Four main parameters have been found to influence the composite physical properties improvement: the fillers content, the physical structure of the polymeric matrix, the particles dispersion and the physical interaction strength between organic and inorganic phases. The dynamic mechanical properties of this biomimetic nanocomposite were compared with human cortical bone.

Keywords: polyamide 6,9; hydroxyapatite; nanocomposite; dynamic mechanical properties; biomimetic

INTRODUCTION

Over the last century, metallic implants as fixation devices and fracture healing have been widely used in orthopaedic surgery as bone substitutes.^{1,2} Clinical studies reported that metallic implants, which are stiffer than calcified tissues, induce a shielding of mechanical stresses in bone, and thus, a resorption phenomenon.^{1,3–6} This is known as Wolff's Law, that is, the bone grows/resorbs in response to mechanical environment and can produce an anatomical structure which is now able to resist to the applied stress.⁷ The difference in the mechanical properties between metallic implants and bone is partly responsible for loosening of rigid prosthesis (a common problem linked to a total hip replacement) and for osteolysis (a complication occurring when rigid fixations are used for fracture).

With their viscoelastic properties, polymeric materials might have modulus of the order of gigapascals with damping effect like bone. As the mechanical environment varies with the implantation site, it is interesting to design materials with well fitting mechanical properties. When the required mechanical modulus remains mild, polymers based on polylactic acid have been successfully designed: in that kind of application we might find bioresorbable materials. Contrarily, when higher modulus is necessary, only nonresorbable materials might fit the mechanical requirements. The modulus will be adapted by adjusting filler rate, and physico-chemical structure of the polymeric matrix.

With this aim, polymer-based composites were widely investigated.^{8–12} The use of high content of inorganic fillers has proven to greatly optimize the mechanical strength of polymers. Filler dispersion, size, and shape, and also quality of dispersion and interfacial bond strength were taken into account to promote mechanical properties and load transfer. However, with high filler content, it becomes diffi-

cult to prevent aggregation. Aggregates are believed to be responsible for stress concentration phenomena, supporting internal cracks, decreased mechanical properties, and thereby damage of composites.⁸ Low filler contents overcome this problem. But, in order to maximize mechanical properties with such low ratio, nanosized particles have to be synthesized.

The use of nanohydroxyapatite in polyamide has been investigated to develop semi-rigid implant materials. The preparation and characterization of these nanocomposites are studied in this work. Hydroxyapatite particles have already been used as fillers to promote the mechanical properties and the bioactivity in physiological conditions^{13–17} of composites. Polyamides are biocompatible polymers due to their chemical similarity to amino acid. They can be processed with specific shapes (e.g. plate, needle-like) for application in orthopedics. Then, the dynamic mechanical impedance of the implant might be adapted to the site. A few researches have been carried out to extend their applications in biomedical fields.^{18–20}

Polyamide 6,9 has been chosen for three reasons: (a) an odd number of carbon atoms in its constitutive unit is responsible for its electroactive properties that might improve osteogenesis; (b) its glass transition temperature is slightly above (by 5–10°C) that of one of more the common polyamides, polyamide 11.

The use of hybrid nanocomposites is one of the methods to improve the mechanical properties of polymer. The synergy between organic and inorganic phases helps us to increase the mechanical modulus of polyamide near the glass transition. In order to check this point, a thorough study was performed on the raw materials (nanohydroxyapatite and polyamide 6,9). Then the evolution of mechanical properties of nanocomposites as a function of nanohydroxyapatite content was studied. We focus on the low frequency dynamic mechanical properties corresponding to dynamic physiological stresses. Since the response is independent of the solicitation mode (tensile, shear, bending, compression), shear mode has been chosen. Finally, we propose an interpretation at a molecular level and shed some light on the way to improve such hybrid nanocomposites.

MATERIALS AND METHODS

Raw Materials, Nanocomposites, and Bones

Hydroxyapatite nanocrystals ($\text{Ca}_{10}(\text{PO}_4)_6(\text{OH})_2$ – space group $\text{P6}_3/\text{m}$) stabilized in a solution of ethanol were synthesized and provided by Berkeley Advanced Biomaterials. Polyamide 6,9 was purchased from Sigma Aldrich and *N,N*-dimethylacetamide (DMAc) solvent was from Prolabo. Composites were prepared by thermally induced phase separation as follows. First, a nHap suspension in DMAc was obtained by a solvent substitution technique: ethanol was removed from the suspension at 75°C while DMAc was dropped into it. Then, to ensure a good dispersion of nHap

particles, ultrasonic irradiation (ultrasonic bath, 30 min) was applied. The system was heated at 145°C under stirring, polyamide pellets were poured into the suspension, and dissolution was done for 3 h. The viscous medium was quenched and washed with distilled water to precipitate the composite, and DMAc was removed. The solid was dried at 170°C under vacuum for 24 h and then crushed for analyses. The bone samples studied in the last part of this work were obtained from the mid-diaphysis of bovine and human femurs.

Methods

Standard analysis techniques such as X-ray diffraction (XRD) in $\theta/2\theta$ configuration, scanning electron microscopy (JEOL JSM 6700F) with field emission gun (SEM-FEG) at 15 kV were used to measure the mean size of nHap particles. XRD diffractogram of nHap crystallites and the Sherrer formula²¹ gave the mean size L_{hkl} of crystallites perpendicular to the (hkl) planes:

$$L_{\text{hkl}} = \frac{K \times \lambda}{\cos \theta \times \beta} \quad (1)$$

with $K \approx 0.94$, the Sherrer constant value; λ , wavelength of X-ray ($\text{CoK}_\alpha = 1.78892 \text{ \AA}$); θ , diffraction angle of (hkl) planes; $\beta = \sqrt{\Delta_r^2 - \Delta_0^2}$, the β factor, the width of the reflection taking into account the instrument correction.

Furthermore, in order to determine the structure of the composite, investigations were made by using high resolution transmission electron microscopy (HRTEM). Electron transparent samples were required. This was achieved by preparing thin foils of nanocomposites (nanohydroxyapatites and polyamide matrix) using diamond ultramicrotomy. The specimens were deposited on copper grids coated with lacey-carbon film. The TEM and HRTEM imaging were performed using a FEI TECNAI F20 S-TWIN. The diffraction patterns were obtained using the selected area diffraction (SAED) mode or by Fourier transform of the HRTEM imaging.

Thermal analyses were carried out on composites: Thermal gravimetric analyses (TGA) to determine the nHap content and standard differential scanning calorimetry (DSC) to study the fillers influence on the physical properties of PA 6,9. DSC measurements were performed using a DSC/TMDSC 2920 set-up manufactured by TA Instruments. The sample temperature was calibrated using the onset of melting of tin ($T_m = 231.8^\circ\text{C} \pm 0.1^\circ\text{C}$), indium ($T_m = 156.6^\circ\text{C} \pm 0.1^\circ\text{C}$), and cyclohexane ($T_m = 6^\circ\text{C}$) with a heating rate of $q_h = 5^\circ\text{C min}^{-1}$. The heat flow was calibrated with the melting enthalpy of indium ($\Delta H = 28.5 \pm 0.1 \text{ J g}^{-1}$); its baseline was corrected with sapphire. For each sample, the glass transition temperature range and also the enthalpy of melting ΔH_m were measured. The glass transition T_g was then defined as the midpoint of the heat capacity change in the heating run.

The most straightforward manner to evaluate the modification in the viscoelastic behaviour is to measure the mechanic relaxation mode of a sample using the constant frequency—constant amplitude temperature scan method. The storage modulus and the loss tangent of the blank and nHap reinforced polyamide system were measured as function of temperature. Dynamic mechanical analyses (DMA) were performed using an ARES (advanced rheometric expansion system) strain controlled rheometer (TA Instruments) in the torsion rectangular mode within the linear elasticity range. Dynamic mechanical storage modulus G' and loss factor $\tan \delta$ were recorded as function of temperature and nHap content from -150°C to 125°C at $3^{\circ}\text{C min}^{-1}$, for $f = 1 \text{ Hz}$ (the equivalent physiological frequency).

These physical and chemical experiments allowed us to investigate the nanocomposite and its components, from nanometric to mesoscopic scale.

RESULTS

Characterization of Raw Materials

Nanohydroxyapatite Characterization. The nHap powder was studied by XRD. The diffractogram shown in Figure 1 shows very narrow peaks, which are characteristic of highly crystallized nHap particles. The mean size was evaluated to 190 nm in the [002] direction, and 60 nm in the [310] direction, using to the Sherrer formula. The SEM picture showed in Figure 2 was recorded on a nHap suspension after liquid phase evaporation. Single needle-like crystals of nHap and also some aggregates (in which crystallites are lying side by side) were pointed out in the commercial solution. The mean dimensions of nanocrystals were $\sim 100\text{--}200 \text{ nm}$ (length) and $40\text{--}60 \text{ nm}$ (width), which are in good correlation with X-ray measurements.

Nanohydroxyapatite particles were synthesized in solution. Aggregation phenomenon could not be totally controlled on a large time scale. Furthermore, the surface energy of nanoparticles tends to decrease with particles

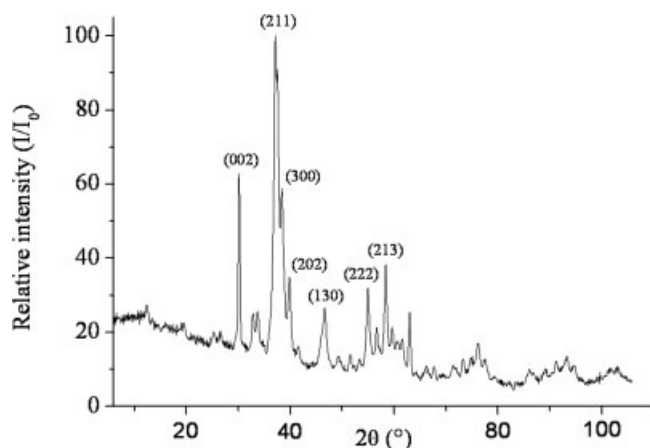


Figure 1. X-ray diffractogram of nanohydroxyapatite powder.

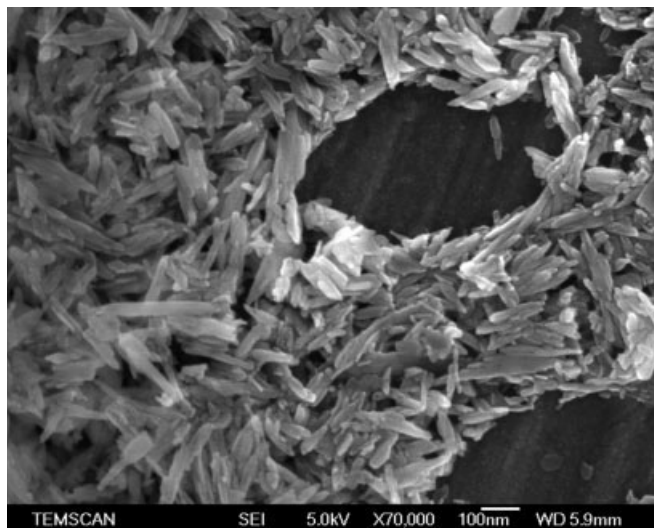


Figure 2. Nanohydroxyapatite single acicular crystals observed by scanning electron microscopy.

aggregation. So, ultrasonic irradiation was applied to the suspension during composites synthesis to prevent them from aggregation. nHap particles retained their nanometer size in ethanol.

Polyamide Matrix Characterization. Differential scanning calorimetry was performed in order to determine the physical structure of polyamide 6,9, shown in Figure 3 by bold line. Two consecutive thermograms were recorded from 0°C to 250°C with a heating rate of $q_h = 10^{\circ}\text{C min}^{-1}$. The glass transition temperature, T_g , measured at heat capacity step, was $T_g = 33.9^{\circ}\text{C}$ (first scan). An endothermic signal is superimposed. This signal is attributed to the disruption of physical bonds formed between amide groups in the vitreous state. A cold crystallisation process occurs at $T_c = 190^{\circ}\text{C}$, before the melting of crystalline phase at $T_m = 210^{\circ}\text{C}$. On the second scan (thermograms are plotted in Figure 3) obtained after cooling the sample from an equilibrium temperature $T_m + 40^{\circ}\text{C}$ to low temperature $T_g - 40^{\circ}\text{C}$, the glass transition temperature was determined at $T_g = 39^{\circ}\text{C}$ ($\Delta C_p = 0.38 \text{ J g}^{-1}\text{C}^{-1}$). The endothermic peak had vanished. This phenomenon is known as physical ageing, which has been already reported in linear²² and complex polymers.²³ The crystallinity ratio χ_c was calculated from the enthalpy of melting recorded during the second scan (ΔH_m), the enthalpy of melting for 100% crystallized PA 6,9 ($\Delta H_{\infty} = 257.4 \text{ J g}^{-1}$ from Athas database), and the cold crystallization enthalpy (ΔH_c).

$$\chi_c = \frac{\Delta H_m - |\Delta H_c|}{\Delta H_{\infty}} \times 100 \quad (2)$$

The crystallinity ratio χ_c for the virgin sample was 16.2%. Evolution of χ_c data as a function of nHap content is discussed in the next section. After the characterization of nHap and polyamide, we investigated the properties of the polymer-based materials.

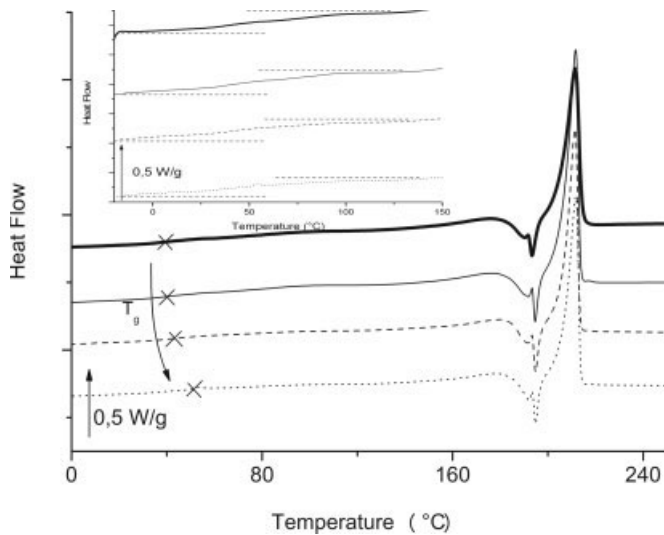


Figure 3. DSC thermograms of polyamide/nanohydroxyapatite composite as a function of nanohydroxyapatite content (PA bold line, PA/nHAP 1% solid line, PA/nHAP 5% dashed line, PA/nHAP 10% dotted line). Details of glass transition temperature range in inset.

Characterization of Polyamide/Nanohydroxyapatite Composites

Dispersion of Nanohydroxyapatite. The TEM imaging of the PA/nHap (Figure 4) shows needle-like nanoparticles of hydroxyapatite embedded in a polyamide matrix. The right part (a) of Figure 4 is characteristic of a thick area where it is very difficult to evaluate the agglomeration degree of nHap, whereas the left part (b) corresponds to a thin area where nanohydroxyapatites in black contrast are clearly surrounded by polymeric matrix (light contrast). The thin and thick areas depend on the ultramicrotomy preparation, the section we obtained being not homogeneous in thickness. Nevertheless, the selected area diffraction

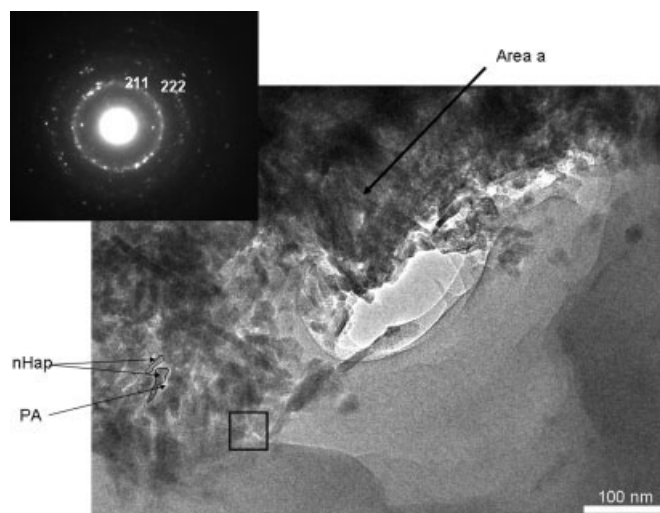


Figure 4. TEM imaging of the composite (nHap/PA). In inset the selected area diffraction pattern obtained on the left area is delimited by a dashed line. A box where the HRTEM imaging was done is also represented.

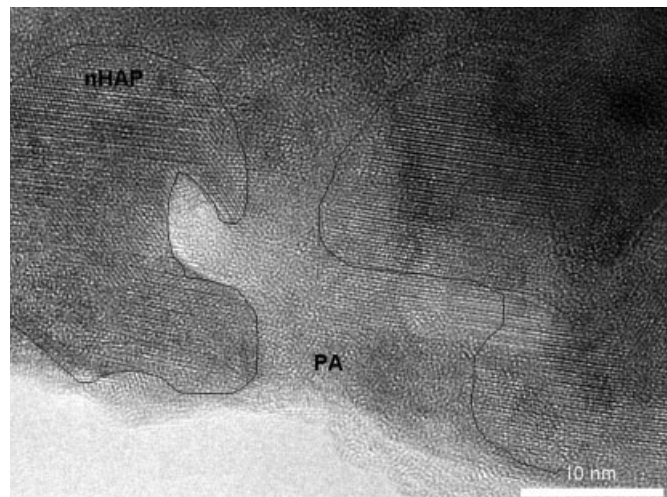


Figure 5. HRTEM imaging of one part of Figure 4 (which is schematized by a box in Figure 4).

(SAED) pattern of the left area delimited by dashed line (in inset of Figure 4) shows well-defined rings which can be easily indexed as nanohydroxyapatites (space group $P6_3/m$). This particular SAED pattern indicates that nHap particles are dispersed in all the directions. The HRTEM imaging of one part of the left area (schematized by a box in Figure 4) displays two well-crystallized nanoparticles of Hap which are surrounded by amorphous matrix (Figure 5). So the dispersion of nanohydroxyapatites in the polymeric matrix is well-achieved without amphiphilic molecules.

Thermal Stability. Nanocomposites were prepared with a nHap content ranging from 0 to 10 wt %. A first mass loss of 1–3% is recorded from 0°C to 150°C. It has been attributed to the desorption of water. The main mass loss between 250°C and 520°C corresponds to the degradation of polymer bulk matrix (Figure 6). Thanks to residue,

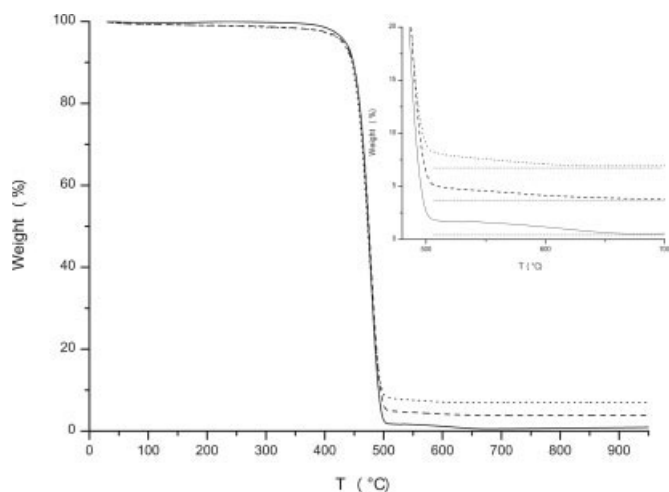


Figure 6. Thermogravimetry thermograms of polyamide nanohydroxyapatite composite as a function of nHap content (PA/nHAP 1% solid line, PA/nHAP 5% dashed line, PA/nHAP 10% dotted line). In inset is the selected temperature range of 450–700°C.

TABLE I. Glass Transition Temperature and Crystallinity Rate of Composites as a Function of Hap Content

nHap Content (%)	Corrected nHap Content (%)	T_g (°C)	T_m (°C)	ΔH_m (J g ⁻¹)	ΔH_c (J g ⁻¹)	χ_c (%)
0	0	39.1	211.4	49.7	8.1	16.2
1	2	39.1	211.7	56.9	8.1	19
5	6	40.7	211.4	52.2	7.8	17.2
10	9	52.1	211.7	44.4	7.6	14.3

nHap content is checked for the series of samples. TGA patterns have shown a good correlation between theoretical and experimental values (called corrected values in Table I). These experiments allow us to check the validity and the stability of our dispersion technique. Beyond 520°C till 650°C, a slight mass loss is observed (Figure 6 inset). This is probably due to the degradation of polyamide shell on nHap particles. Indeed, macromolecules that are surrounded by particles might be more strongly bonded to nHap. Such a configuration requires more energy to be dissipated.²⁴

Physical Structure of Polyamide. DSC thermograms of the nanocomposites shown in Figure 3 show three main thermal phenomena: the glass transition temperature near 45°C, a cold crystallization before 200°C, and a melting at 210°C. An increase of the glass transition temperature is recorded upon increasing of nHap ratio. By raising the mass fraction of inorganic fillers from 0% to 10%, T_g increases from 39.1°C to 52.1°C. The dispersion of nHap particles promotes the physical interactions with polyamide groups. The crystallinity rate of this composite is reported on Table I. The crystallinity rate of polyamide has been calculated from true value of ΔH_m and ΔH_c (normalized by the polymer mass). The evolution of crystallinity is not clearly dependent on nHap ratio. Fillers do not play the role of seeds for crystallization process. But for high nHap content, crystallinity value falls lower than virgin PA 6,9.

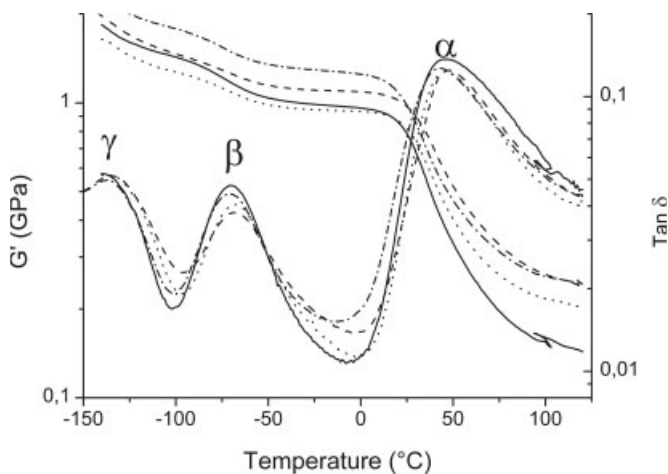


Figure 7. Evolution of G' and $\tan \delta$ thermograms as function of nanohydroxyapatite content at 1 Hz (PA solid line, PA/nHAP 1% dashed line, PA/nHAP 5% dashed dotted line, PA/nHAP 10% dotted line).

So the nHap content optimized for the nHap/polyamide nanocomposites is lower than 5%.

Dynamic Mechanical Properties. The storage modulus and the loss tangent of the blank and nHap reinforced polyamide systems are measured as function of temperature; results are reported in Figure 7. Three relaxation processes are pointed out: the α relaxation mode near 47°C associated with the mechanical manifestation of the glass transition, the β mode near -72°C characteristic of the free amide group/water complex movements, and near -137°C the local γ mode due to aliphatic sequences motions. These mechanical relaxation modes have been observed and discussed by several authors.²⁵

The magnitude and temperature position of these three peaks are not significantly modified by addition of nHap fillers. Thus, the mobility of relaxing entities in amorphous phase is not directly altered by low nHap content.

In Figure 7, we report an increase in the storage modulus for 1 and 5 wt % nHap samples, as we compared to the response of the pure polyamide sample at both low and high temperatures. The storage moduli values for each sample at 0°C and 100°C are compared in Table II. Concerning the mechanical storage modulus G' at 0°C, an increase of 30% is recorded till 5% in weight of nHap: G' increases from 0.96 to 1.25 GPa. For 10% of nHap, G' decreases below the initial value. The loss modulus G'' has been also plotted in Figure 8 as a function of nHap content. A broadening is observed for β and α relaxation modes. It is necessary to compare these results the mechanical behaviour of bone in the same experimental conditions. G' and $\tan \delta$ thermograms of bovine bone and human bone at 1 Hz are indicated in Figure 9. If we compare the mechanical storage modulus G' at the physiological temperature for bovine and human bones, we observe that G' for bovine bone is 10 times higher than that for human bone. This point will be discussed later.

TABLE II. Comparison of Storage Modulus for Polyamide-Based Samples

	G' at 0°C (GPa) Vitreous Plateau	G' at 100°C (GPa) Rubbery Plateau
PA	0.960	0.154
1% nHap in weight	1.089	0.262
5% nHap in weight	1.251	0.258
10% nHap in weight	0.935	0.217

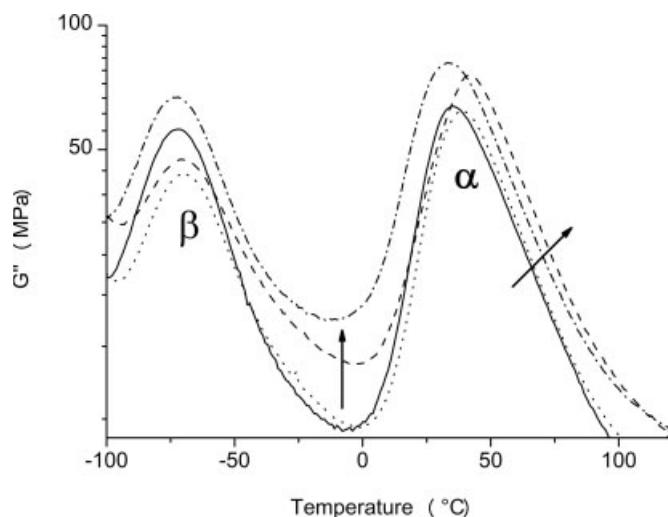


Figure 8. Evolution of G'' thermograms as function of nano-hydroxyapatite content at 1 Hz (PA solid line, PA/nHAP 1% dashed line, PA/nHAP 5% dashed dotted line, PA/nHAP 10% dotted line).

DISCUSSION

In this work, the physical behaviour of polyamide 6,9/nHap nanocomposites has been analyzed. The nanosize of the inorganic filler is checked by XRD (Figure 1) and SEM (Figure 2). As shown by DSC thermograms (Figure 3), the glass transition temperature T_g of nanocomposites increases ($\sim 10^\circ\text{C}$) for increasing rate of nano-hydroxyapatite (1 to 10 wt %). The physical structure of the amorphous phase of polyamide, which is stabilized by hydrogen bonds, is reinforced by nHap. Moreover, interactions between amide groups of polyamide and surface hydroxyl groups of nHap have been detected by FTIR spectrometry. It is interesting to note here that such an increase of the glass transition temperature has also been identified in nanocomposites with carbon nanotubes CNT as filler either with a thermoplastic matrix²⁶ or a thermoset matrix,²⁷ for CNT content lower than the percolation threshold. Such a phenomenon is observed for optimized dispersion. This critical point has been confirmed by TEM (Figure 4) and HRTEM (Figure 5).

At the glass transition, the delocalized molecular mobility of polyamide sequences in the amorphous phase is liberated. This mobility is also responsible for the primary relaxation mode α , so that it is interesting to compare T_g with T_α , the maximum of this energy loss peak. As can be seen in Figure 8 in the thermogram of G'' corresponding to the smaller percentage of nHap, the α peak is shifted towards higher temperatures. This result is coherent with the evolution of T_g (Table I) and it confirms the existence of interactions between nHap and amide groups in the amorphous phase (previously observed by TGA in Figure 6 inset).

Both the storage moduli and the loss tangent thermograms of nanocomposites show a slight broadening of the viscoelastic response, which is most evident in the loss

moduli peak on Figure 8. This broadening occurs predominantly on the high temperature side of the peaks; this suggests that nHap increases the heterogeneity of the amorphous phase towards regions of lower molecular mobility. The stiffening of polymeric interphases in the vicinity of nano-hydroxyapatite might be responsible for this evolution.

Now, let us consider the evolution of the glassy moduli observed (Figure 7) in the thermogram of the conservative moduli G' , on the low temperature side. Up to 5 wt % of nano-hydroxyapatite, the mechanical modulus of nanocomposites increases ($G' = 1.0 \text{ GPa}$ at 37°C); above 5 wt %, G' decreases. The evolution of the magnitude of the dissipative moduli G'' , presented on Figure 8, confirms the evolution of G' . These observations can be related to an evolution of the crystallinity rate: the analysis of the melting peak observed in DSC shows an increase of PA crystallinity for lower content of nHap and a decrease over this threshold (Table II). Above 5%, another factor has to be taken into account: the aggregation phenomenon of nHap, which might induce internal cracks and reduce mechanical properties. *De facto* amphiphilic molecules have been used for preventing aggregation. This method has been already used for the dispersion of carbon nanotubes.²⁸ But no improvement of mechanical properties of nanocomposites was reported and this method was abandoned. Furthermore, there is a risk of plasticization of the polymeric matrix by amphiphilic molecules. So, the dispersion of nanoparticles in polyamide has been achieved without amphiphilic molecules.

In vivo, this biomaterial will work at the physiological temperature; so the mechanical behaviour of this nanocomposite will be located in its viscoelastic range, which is interesting because reversible dissipative effects are operative, but critical since it implies a decrease of the conservative moduli till some 0.8 GPa.

In order to compare nanocomposites with calcified tissue, mechanical experiments were carried out on human and bovine femurs using a similar procedure, at the physio-

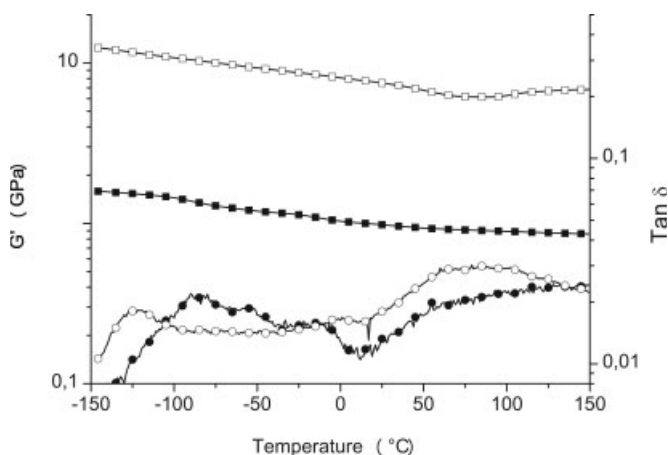


Figure 9. G' (square) and $\tan \delta$ (circle) thermograms of bovine bone (open symbols) and human bone (filled symbols) at 1 Hz.

logical frequency (1 Hz); the data are reported in Figure 9. Mechanical storage modulus G' at 37°C decreases from 7.00 GPa for bovine femur to 1.00 GPa in the case of human femur. It is interesting to compare the mechanical storage modulus value of the human femur with the value measured by Garner et al.,²⁹ at 3.42 GPa. The difference between both values might be due to the pathological nature of the human femur (osteoporosis). Indeed, as indicated in already published studies,³⁰ osteoporosis is responsible for a decrease of cortical bone modulus. If we compare the mechanical storage modulus G' at the physiological temperature for bone and for the nanocomposite, we note that they remain of the same order of magnitude so that, by playing with the morphology of the biomaterial, we may attain the required rigidity.

It also important to consider the loss modulus of bone at the physiological temperature with the one of nanocomposites: both are viscoelastic with a dissipative effect of the same order of magnitude. Consequently, they exhibit analogous damping phenomena insuring their biocompatibility on a mechanical point of view and also their ductility.

CONCLUSION

The aim of this research was to contribute to the development of biomimetic organic/inorganic nanocomposites with dynamic mechanical properties similar to those of calcified tissue. The introduction of nHap at a content lower than 5 wt % increases the PA 6,9 crystallinity ratio, and consequently the mechanical modulus on the glassy elastic plateau. The decisive character of dispersion state was also pointed out. Indeed, aggregation phenomena of fillers limit the increase of the mechanical properties in reinforced polymeric materials. Hydrogen bonds at the nHap-PA interface have been detected between amide groups of polyamide and surface hydroxyl groups of nHap, by FTIR spectroscopy. This is a promising mechanism for the development of load transfers from matrix to nanofillers in polyamide/nHap composites. Nanohydroxyapatite is evidently efficient nanofiller for the reinforcement of polymeric composites.

At physiological frequency and temperature, the nanocomposite with lower nHap content (1 wt %) exhibit an elastic behaviour with a conservative modulus of the same order of magnitude than cortical bone. It can be considered as a structural biomaterial. Moreover, with its viscoelastic behaviour characterized by a dissipative modulus analogous with the one of calcified tissues, it is also a damping material mechanically biocompatible, in dynamic conditions.

It looks essential to check the dynamic mechanical behaviour of this nanocomposite in wet environment. Dynamic mechanical analysis in physiological conditions (37°C, 1 Hz, in physiological liquid) is under investigation. In order to cover a broader range of application sites requiring higher modulus on the glassy plateau, new semi-aromatic polyamide matrices are also studied. In the long term, such nanocomposites could be used in load-bearing

applications where nonbioabsorbable implants with high dynamic mechanical moduli are needed, for example, as intersomatic cages for spinal arthrodesis or as osteosynthetic plates in fracture healing.

The authors thank Elisabeth Laurent, Isabelle Savin de Larclause, and Marc Cantagrel for very helpful preliminary work.

REFERENCES

1. Park JB, Lakes RS. *Biomaterials: An Introduction*, 2nd ed. New York: Plenum; 1992.
2. Helsen JA, Breme HJ. *Metals as Biomaterials*. Chichester: Wiley; 1998.
3. Bradley GW, McKenna GB, Dunn HK, Daniels AU, Statton WO. Effects of flexural rigidity of plates on bone healing. *J Bone Joint Surg A* 1979;61:866-872.
4. Paavolainen P, Karaharju E, Slätis P, Ahonen J, Holmström T. Effect of rigid plate fixation on structure and mineral content of cortical bone *Clin Orthop Relat Res* 1978;136:287-293.
5. Aro H, Eerola E, Aho AJ. Osteolysis after rigid fixation. *Clin Orthop Relat Res* 1982;166:292-300.
6. Uthoff HK, Finnegan M. The effects of metal plates on post-traumatic remodelling and bone mass. *J Bone Joint Surg B* 1983;65:66-71.
7. Wolff JD. *Das gesetz der transformation der knochen* Hirschwald Berlin 1982. Berlin: Springer; 1987 (reprinted, english translation).
8. Wang M. Developing bioactive composite materials for tissue replacement. *Biomaterials* 2003;24:2133-2151.
9. Wetzel B, Hauptert F, Zhang MQ. Epoxy nanocomposites with high mechanical and tribological performance. *J Compos Sci Technol* 2003;63:2055-2067.
10. Zhang Q, Archer LA. Poly(ethylene oxide)/silica nanocomposites: Structure and rheology. *Langmuir* 2002;18:10435-10442.
11. Reynaud E, Jouen T, Gauthier C, Vigier G, Varlet J. Nanofillers in polymeric matrix: A study on silica reinforced PA6. *Polymer* 2001;42:8759-8768.
12. Yang F, Ou Y, Yu Z. Polyamide 6/silica nanocomposites prepared by in situ polymerization. *J Appl Polym Sci* 1998;69:355-361.
13. Cheang P, Khor KA. Effect of particulate morphology on the tensile behaviour of polymer-hydroxyapatite composites. *Mater Sci Eng A* 2003;345:47-54.
14. Roeder RK, Sproul MM, Turner CH. Hydroxyapatite whiskers provide improved mechanical properties in reinforced polymer composites. *J Biomed Mater Res A* 2003;67:801-812.
15. Xu HHK, Quinn JB. Whisker-reinforced bioactive composites containing calcium phosphate cement fillers: Effects of filler ratio and surface treatments on mechanical properties. *J Biomed Mater Res* 2001;57:165-174.
16. Liu Q, de Wijn JR, van Blitterswijk CA. Nano-apatite/polymer composites: Mechanical and physicochemical characteristics. *Biomaterials* 1997;18:1263-1270.
17. Wang M, Bonfield W. Chemically coupled hydroxyapatite-polyethylene composites: Structure and properties. *Biomaterials* 2001;22:1311-1320.
18. Kawai T, Ohtsuki C, Kamitakahara M, Miyazaki T, Tanihara M, Sakaguchi Y, Konagaya S. Coating of an apatite layer on polyamide films containing sulfonic groups by a biomimetic process. *Biomaterials* 2004;25:4529-4534.
19. Huang M, Feng J, Wang J, Zhang X. Synthesis and characterization of nano-HA/PA66 composites. *J Mater Sci Mater Med* 2003;14:655-660.

20. Wang X, Li Y, Wei J, de Groot K. Development of biomimetic nano-hydroxyapatite/poly(hexamethylene adipamide) composites. *Biomaterials* 2002;23:4787–4791.
21. Scherrer P. Estimation of the size and internal structure of colloidal particles by Röntgen rays. *Gött Nachr* 1918;2:98–100.
22. Struik LCE. *Physical Aging in Amorphous Polymers and Other Materials*. Amsterdam: Elsevier; 1978.
23. Dantras E, Dandurand J, Lacabanne C, Caminade AM, Majoral JP. Enthalpy relaxation in phosphorus-containing dendrimers. *Macromolecules* 2002;35:2090–2094.
24. Deng X, Hao J, Wang C. Preparation and mechanical properties of nanocomposites of poly(D,L-lactide) with Ca-deficient hydroxyapatite nanocrystals. *Biomaterials* 2001;22:2867–2873.
25. Varlet J, Cavaillé JY, Perez J, Johari GP. Dynamic mechanical spectrometry of nylon-12. *J Polym Sci B* 1990;28:2691–2705.
26. Yang J, Lin Y, Wang J, Lai M, Li J, Liu J, Tong X, Cheng H. Morphology, thermal stability, and dynamic mechanical properties of atactic polypropylene/carbon nanotube composites. *J Appl Polym Sci* 2005;98:1087–1091.
27. Barrau S, Demont P, Maraval C, Bernès A, Lacabanne C. Glass transition temperature at the percolation threshold in carbon nanotube-epoxy and polypyrrole-epoxy resin composites. *Macromol Rapid Commun* 2005;28:390–394.
28. Barrau S, Demont P, Perez E, Peigney A, Laurent C, Lacabanne C. Effect of palmitic acid on the electrical conductivity of carbon nanotubes-epoxy resin composites. *Macromolecules* 2003;36:9678–9680.
29. Garner A, Lakes R, Lee T, Swan C, Brand R. Viscoelastic dissipation in compact bone: Implications for stress-induced fluid flow in bone. *J Biomech Eng* 2000;122(2):166–172.
30. Aguado F, Revilla M, Villa LF, Rico H. Cortical bone resorption in osteoporosis. *Calc Tissue Int* 1997;60:323–326.